Thermosolutal Inducement of No-Slip Free Surfaces in Combined Marangoni-Buoyancy Driven Cavity Flows

J. R. Keller

T. L. Bergman
Assistant Professor.
Assoc. Mem. ASME

Department of Mechanical Engineering,
The University of Texas at Austin,
Austin, TX 78712

The presence of a diffusing surfactant in combined surface tension-buoyancy driven convection is studied numerically to examine its influence on the flow structure and heat transfer characteristics of a fluid contained within a cavity. By accounting for the surface tension dependence on both temperature and surfactant concentration, the free surface may become stagnant. As a result, the high local and overall heat transfer rates at the cold wall, which are associated with thermal surface tension-augmented buoyancy driven flows, are decreased.

Introduction

Combined surface tension-buoyancy driven convection is relevant in a variety of engineering systems and manufacturing processes. Oftentimes, this type of convection is present within liquid melts in conjunction with melting and solidification heat transfer during, for example, welding (Kou, 1987), glass making (Stanek and Szekely, 1970; McNeil et al., 1985), metals processing (Camel et al., 1986) and crystal growth (Hurle and Jakeman, 1981). As a result, melting and solidification rates as well as the ultimate product quality may be affected by convection driven by simultaneous buoyancy and surface tension forces.

For a pure fluid, variations in the liquid surface tension occur due to its dependence on the liquid temperature. If the thermally induced surface tension variation occurs along a free surface, the net thermocapillary force will either augment or oppose the buoyancy driven flow within the bulk of the liquid layer. As a result, two distinct thermocapillary flow regimes may exist in, for example, a liquid held within a cavity with heated and cooled side walls.

If thermocapillary forces augment buoyancy forces, free surface velocities increase relative to the pure buoyancy case, advection of thermal energy from the upper hot wall to the upper cold wall is enhanced, and very high local heat transfer rates occur near the top of the cold wall (Schwabe et al., 1978; Villers and Platten, 1985; Bergman and Ramadhyani, 1986). In contrast, if opposing thermocapillary forces are present, a bicellular flow structure may result, leading to decreased heat transfer rates relative to the pure buoyancy case (Legros et al., 1984; Villers and Platten, 1985; Bergman and Ramadhyani, 1986). Most real fluids are susceptible to flow behavior of the first regime while only a few fluids exhibit the second type of flow.

While experimental results and numerical predictions indicate that thermocapillary effects exist and can be significant under certain conditions, it is typical of many systems to possess free surfaces characterized by stagnant conditions (Heiple and Roper, 1982; Kirdyashkin, 1984; Platten and Villers, 1987). This type of behavior constitutes a third flow regime and is superficially identical to the pure buoyancy case with an applied no-slip boundary condition at the free surface. As is evident from a force balance along the free surface, however, surface tension forces must remain in effect, since their absence implies applicability of a no-shear hydrodynamic boundary condition and, in turn, finite velocities at the free surface, which are driven by buoyancy-induced flow in the bulk of the fluid. Thermocapillary forces are not negligible in the third flow regime; they must be counterbalanced by an opposing mechanism.

It is well known that trace concentrations of contaminants such as dust, ionic materials, or other liquids can reduce the surface tension of a host liquid (Shinoda, 1963). If the contaminant is a surfactant, concentration gradients may be induced at the free surface in response to advective mechanisms resulting from other driving forces. In turn, the nonuniform concentration distribution produces surface tension gradients at the free surface, which affect convective transport in the bulk liquid.

Coupling between the solutocapillary convection and bulk fluid motion was initially proposed by Levich in 1948 (1962) to describe behavior of air bubbles rising through a stagnant fluid layer. However, the model could not accurately predict the drag force dependence on particle size and a "stagnant cap" model was developed (Savic, 1953). Here, the insoluble surfactants are advected to the rear of the bubble, creating a stagnant region. Davis and Acrivos (1966) were able to employ the stagnant cap model to predict the rise velocity of air bubbles in a liquid layer. As will become evident, a three-way coupling between buoyancy-induced advection, thermocapillary forces, and solutocapillary forces is responsible for the flow of the third regime.

Analysis

In order to understand the coupling process that induces free surface stagnation, the system of Fig. 1 is considered. A host liquid is contained in a cavity of length L and a free surface is present at $y=H$. Fluid motion is induced by imposing appropriate thermal boundary conditions and is due to the presence of buoyancy and surface tension forces within the bulk fluid and at the free surface, respectively.

By assuming a flat, nondeformable free surface and steady, laminar two-dimensional flow with negligible viscous dissipation, the governing equations for the Boussinesq host liquid are:

$$\frac{\partial u}{\partial x} + \frac{\partial v}{\partial y} = 0 \tag{1}$$

Contributed by the Heat Transfer Division for publication in the JOURNAL OF HEAT TRANSFER. Manuscript received by the Heat Transfer Division November 27, 1988; revision received June 19, 1989. Keywords: Double Diffusion Systems, Enclosure Flows, Thermocapillary Flows.

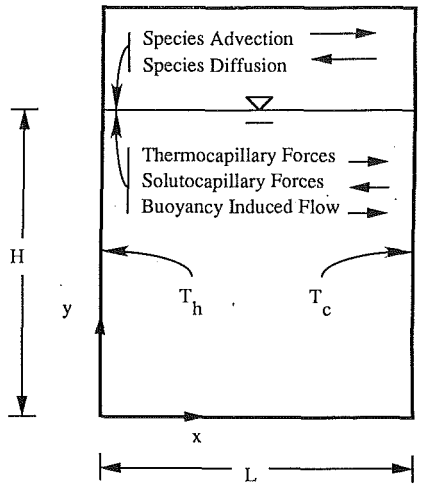

Fig. 1 Schematic of the system showing buoyancy and surface tension forces and surface species diffusion

$$\frac{\partial}{\partial x}(uu)+\frac{\partial}{\partial y}(uv)=\frac{\partial}{\partial x}\left(\nu\frac{\partial u}{\partial x}\right)+\frac{\partial}{\partial y}\left(\nu\frac{\partial u}{\partial y}\right)-\frac{1}{\rho}\frac{\partial P}{\partial x} \tag{2}$$

$$\frac{\partial}{\partial x}(vu)+\frac{\partial}{\partial y}(vv)=\frac{\partial}{\partial x}\left(\nu\frac{\partial v}{\partial x}\right)+\frac{\partial}{\partial y}\left(\nu\frac{\partial v}{\partial y}\right)-\frac{1}{\rho}\frac{\partial P}{\partial y}+g\beta(T-T_o) \tag{3}$$

$$\frac{\partial}{\partial x}(uT)+\frac{\partial}{\partial y}(vT)=\frac{\partial}{\partial x}\left(\alpha\frac{\partial T}{\partial x}\right)+\frac{\partial}{\partial y}\left(\alpha\frac{\partial T}{\partial y}\right) \tag{4}$$

If a surfactant is present along the free surface, it will be subjected to horizontal advection associated with the flow in the host liquid. Horizontal diffusion of the surfactant opposes its advective transport.

$$\frac{\partial}{\partial x}(uc)\Big|_{y=H}=\frac{\partial}{\partial x}\left(D\frac{\partial c}{\partial x}\right)\Big|_{y=H} \tag{5}$$

The hydrodynamic boundary conditions include no-slip conditions at the cavity walls and bottom. The hydrodynamic conditions at $y=H$ result from a force balance at the free surface (Levich and Krylov, 1969)

$$\mu\frac{\partial u}{\partial y}\Big|_{y=H}=\sigma_T'\frac{\partial T}{\partial x}\Big|_{y=H}+\sigma_c'\frac{\partial c}{\partial x}\Big|_{y=H} \tag{6}$$

and

$$v\Big|_{y=H}=0 \tag{7}$$

The thermal boundary conditions considered in this study are

$$T=T_h\Big|_{x=0},\qquad T=T_c\Big|_{x=L} \tag{8}$$

and

$$\frac{\partial T}{\partial y}\Big|_{y=0,H}=0 \tag{9}$$

The surfactant concentration boundary conditions are

$$\frac{\partial c}{\partial x}\Big|_{x=0}=\frac{\partial c}{\partial x}\Big|_{x=L}=0 \tag{10}$$

with the constraint

$$\frac{1}{L}\int_{x=0}^{x=L}c(x)dx=c_{\text{avg}} \tag{11}$$

where c_{avg} is specified a priori.

In writing equations (5) and (11), it is assumed that the contaminant is limited to a thin film, which rides upon the free surface. Inspection of equation (10) reveals that, if a surface velocity exists, the surfactant will be trapped against one of the enclosure walls and its diffusion will induce a concentration gradient along the free surface. The presence of the surfactant eventually influences bulk convective flow and heat transfer in the host liquid through the Marangoni hydrodynamic boundary condition, equation (6).

The following dimensionless parameters govern the system behavior and are identified by appropriate normalization of the governing equations and applied boundary conditions.

Rayleigh number	$\text{Ra}=g\beta\Delta TL^3/\nu\cdot\alpha$	(12)
Prandtl number	$\text{Pr}=\nu/\alpha$	(13)
Schmidt number	$\text{Sc}=\nu/D$	(14)
thermal Marangoni number	$\text{Ma}_T=\sigma_T'\Delta TL/\mu\cdot\alpha$	(15)
solutal Marangoni number	$\text{Ma}_c=\sigma_c'c_{\text{avg}}L/\mu\cdot\alpha$	(16)
liquid layer aspect ratio	$A=H/L$	(17)

It should be noted that the average surfactant concentration is used to normalize the concentration in equations (5), (6), and

Nomenclature

A = liquid layer aspect ratio $=H/L$
Bo = dynamic Bond number $=\text{Ra}/\text{Ma}_T$
c = specific heat, surfactant concentration
D = species diffusion coefficient
E = elasticity number $=\text{Ma}_c/\text{Ma}_T$
g = gravitational acceleration
h = local heat transfer coefficient
H = height of the liquid layer
k = thermal conductivity
L = width of the liquid layer
Le = Lewis number $=\text{Sc}/\text{Pr}$
Ma_c = solutal Marangoni number $=\sigma_c'c_{\text{avg}}L/\mu\cdot\alpha$
Ma_T = thermal Marangoni number $=\sigma_T'\Delta TL/\mu\cdot\alpha$
$\underline{\text{Nu}}$ = local Nusselt number $=hL/k$
$\overline{\text{Nu}}$ = average Nusselt number $=H^{-1}\int_{y=0}^{y=h}\text{Nu}\,dy$
p = pressure
Pr = Prandtl number $=\nu/\alpha$
Ra = Rayleigh number $=g\beta\Delta TL^3/\nu\cdot\alpha$
Sc = Schmidt number $=\nu/D$
T = temperature
u = horizontal velocity
u^* = dimensionless horizontal velocity $=uL/\alpha$
v = vertical velocity
x = horizontal coordinate
y = vertical coordinate
α = thermal diffusivity $=k/\rho\cdot c$
β = thermal expansion coefficient
μ = dynamic viscosity
ν = kinematic viscosity
ρ = mass density
σ' = surface tension variation with temperature or concentration
ψ = dimensionless streamfunction

Subscripts

c = concentration, cold
h = hot
max = maximum
min = minimum
o = reference
T = thermal

(10) due to the absence of a characteristic concentration difference in the system.

Three additional dimensionless parameters may be derived from equations (12)–(17). Although they are not independent they are useful to consider,

Lewis number $\quad \mathrm{Le} = \mathrm{Sc}/\mathrm{Pr} = \alpha/D \quad (18)$

dynamic Bond number $\quad \mathrm{Bo} = \mathrm{Ra}/\mathrm{Ma}_T = g\beta\rho L^2/\sigma_T' \quad (19)$

elasticity number $\quad E = \mathrm{Ma}_c/\mathrm{Ma}_T = c_{\mathrm{avg}}\sigma_c'/\Delta T \cdot \sigma_T' \quad (20)$

The Lewis number is the ratio of thermal to species diffusivities while the dynamic Bond number describes the relative strength of buoyancy to thermal surface tension forces. The elasticity number is a ratio of solutocapillary to thermocapillary forces and has been used previously to describe the influence of a nondiffusing surfactant on surface-tension induced flow (Homsy and Meiburg, 1984; Carpenter and Homsy, 1985).

Solution Technique

The governing equations for the host liquid were discretized using the control volume methodology and the power-law scheme was employed to predict the control surface quantities of the advection-diffusion equations (Patankar, 1980). The SIMPLER algorithm was used to predict the pressure field (Patankar, 1980). The governing equation for the surfactant concentration distribution (5) was solved at every iteration by employing the power law approximation to the exact solution of the one-dimensional advection-diffusion equation.

A grid dependence study has shown that a 40×70 (vertical by horizontal) grid network with packed grids along the free surface and cavity walls is adequate to insure grid independent results for the surfactant concentration and surface velocity distributions, as well as the flow structure in the bulk of the fluid and the local and overall heat transfer rates. The grid packing scheme decreases the dimensions of the control volumes by 10 percent as one progresses from the cneter of the computational domain. The buoyancy portion of the model was validated by comparing the predicted heat transfer rates across a square air-filled cavity with heated endwalls to a benchmark numerical solution (De Vahl Davis, 1983). Average Nusselt numbers were within 2 percent of the benchmark predictions to $\mathrm{Ra} = 10^6$. The surface tension portion of the model was compared to predictions for pure surface tension flow in a square cavity with heated end walls (Zehr et al., 1987). Predicted surface velocities, surface temperatures, and local wall heat fluxes were within 2 percent of the benchmark values for $\mathrm{Ma} \leq 10^3$. It should be noted that the presence of the surfactant significantly reduces the severe grid packing requirements, which are generally necessary to model thermocapillary-induced flow in cavities (Zehr et al., 1987).

Results

Numerical simulations were performed for a range of Ra ($10^2 \leq \mathrm{Ra} \leq 10^6$), Ma_T (250 and 10^3), and E (0.0, 0.1, 0.2, 0.3, ∞). Due to the relative expense of the computations, Pr and A were held at unity while Le values were 1, 10, and 100, which are typical of most host liquids. The value of c_{avg} is 0.001 for all the simulations. The hydrodynamic results are presented in terms of the dimensionless streamfunction, which is defined as

$$\psi(x, y=0) = \psi(x=0, y=0) + \frac{1}{\nu}\int_{x=0}^{x} v\, dx \quad (21)$$

$$\psi(x, y) = \psi(x, y=0) - \frac{1}{\nu}\int_{y=0}^{y} u\, dy \quad (22)$$

with $\psi(x=0, y=0)$ assigned a value of zero.

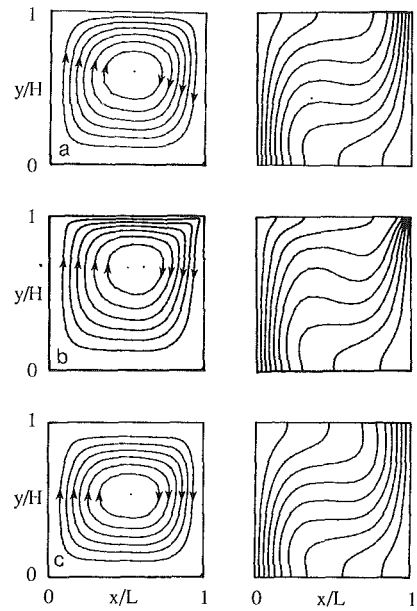

Fig. 2 Predicted streamlines (left) and isotherms (right) for (a) $\mathrm{Ra} = 10^4$, $\mathrm{Ma}_T = 0.0$, $E = 0.0$, $\psi_{\max} = 5990$; (b) $\mathrm{Ra} = 10^4$, $\mathrm{Ma}_T = 10^3$, $E = 0.0$, $\psi_{\max} = 7050$; and (c) $\mathrm{Ra} = 10^4$, $\mathrm{Ma}_T = 10^3$, $E = 0.3$, $\psi_{\max} = 5130$

Predicted Convective Hydrodynamics. Figure 2 shows predicted streamlines and isotherms for no-shear free surface boundary conditions (Fig. 2*a*, $\mathrm{Ra} = 10^4$, $\mathrm{Ma}_T = 0$, $E = 0$), thermocapillary boundary conditions (Fig. 2*b*, $\mathrm{Ra} = 10^4$, $\mathrm{Ma}_T = 10^3$, $E = 0$) and combined thermo-solutocapillary boundary conditions (Fig. 2*c*, $\mathrm{Ra} = 10^4$, $\mathrm{Ma}_T = 10^3$, $E = 0.3$, $\mathrm{Le} = 100$).

Due to the absence of free surface shear in Fig. 2(*a*), surface velocities are nonzero and the center of rotation is slightly above $y/H = 0.5$. Advection of thermal energy is enhanced at $y/H = 1.0$ relative to $y/H = 0.0$ and $\psi_{\max} = 5990$.

Inclusion of buoyancy-augmenting thermocapillary forces at the free surface leads to the flow of the first regime, as shown in Fig. 2(*b*). An effective shear is established at $y/H = 1.0$ by thermally induced surface tension variations at this location, surface velocities are increased substantially, and enhanced advection of warm temperature fluid leads to isotherm compaction at the top of the cold wall. As a result of enhanced free surface velocities, the center of rotation is higher relative to Fig. 2(*a*) and $\psi_{\max}$ is increased to 7050.

Figure 2(*c*) shows the predicted system response as solutocapillary forces, resulting from the presence of the surfactant, counteract thermocapillary forces at the free surface. The streamlines and isotherms bear a remarkable similarity to pure buoyancy flow with imposed no-slip boundary conditions at $y/H = 1.0$. The center of rotation is at $y/H \cong 0.5$, $\psi_{\max}$ is reduced to 5130 and the isotherm distribution is nearly antisymmetric about $x/L = 0.5$.

In order to understand better the coupling responsible for the results of Fig. 2, dimensionless surface velocity and surfactant concentration distributions are presented in Fig. 3.

For the case where no shear exists ($\mathrm{Ma}_T = 0$, $E = 0$, Fig. 2*a*) the dimensionless surface velocity is maximum near $x/L = 0.5$ and the surfactant is pushed to a location adjacent to the cold wall. In contrast, if thermocapillary effects are accounted for ($\mathrm{Ma}_T = 10^3$, $E = 0$, Fig. 2*b*), the free surface velocities are increased everywhere and the isotherm compaction at $x/L \cong 1.0$ leads to substantial thermocapillary-induced velocities near the cold wall. As a result, the surfactant is swept into a very small region adjacent to the cold wall and its distribution has been omitted from Fig. 3 for clarity.

In reality, surfactant concentration gradients resulting from buoyancy and thermocapillarity will induce solutocapillary

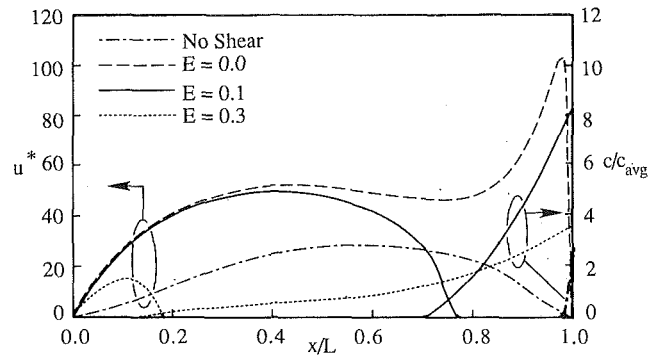

Fig. 3 Dimensionless surface velocity and concentration distributions for the predictions of Fig. 2

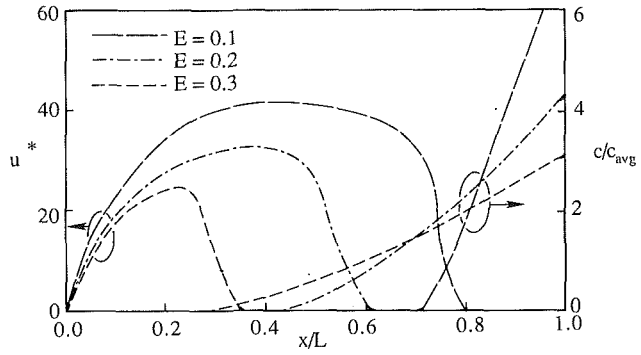

Fig. 5 Dimensionless surface velocity and concentration distributions for the predictions of Fig. 4

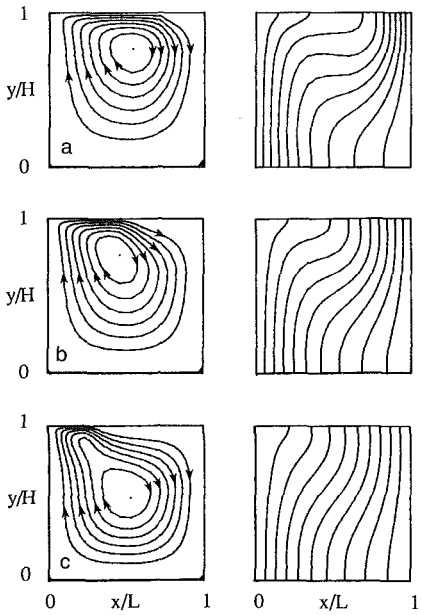

Fig. 4 Predicted streamlines (left) and isotherms (right) for $Ra = 10^3$, $Ma_T = 10^3$, (a) $E = 0.1$, (b) $E = 0.2$, and (c) $E = 0.3$. Values of ψ_{max} are 4100, 2180, and 1300 for $E = 0.1$, 0.2, and 0.3, respectively.

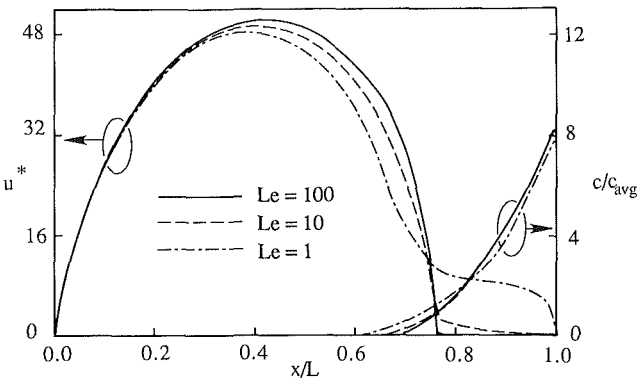

Fig. 6 Dimensionless surface velocity and concentration distributions for various Le; here, $Ra = 10^4$, $Ma_T = 10^3$, and $E = 0.1$

forces that oppose their thermal counterparts (for most liquids). The result is partial or complete surface stagnation. Dimensionless surface velocity and surfactant concentration distributions are included for two nonzero values of E in Fig. 3.

For $Ma_T = 10^3$, $E = 0.1$, the steep concentration gradients resulting from free surface advection induced by buoyancy and/or thermocapillary forces produce surface tension forces at $y/H \cong 1$ as described by equation (6). As a result, surface velocities are decreased near the cold wall, species diffusion extends the surfactants to smaller x/L, and an equilibrium condition is reached where the free surface is stagnant in the range $0.8 \leq x/L \leq 1.0$. Since its magnitude is so small relative to other velocities in the system, the surface velocity distribution in this range is not evident in Fig. 3.

As E is increased further ($Ma_T = 10^3$, $E = 0.3$, Fig. 2c), surfactant concentration gradients wield an even greater influence on the system hydrodynamics and the entire surface is stagnant except for at small x/L. Further increases in E result in an effective free surface no-slip condition at all x/L. The case of total free surface stagnation is typical for many common fluids (see Appendix).

Figure 4 includes predicted streamlines and isotherms that illustrate the role of buoyancy driven flow in the coupling process at the free surface. The dimensionless parameters associated with Fig. 4 are identical to those of Figs. 2 and 3, except Ra is reduced to 10^3 and E values are 0.1, 0.2, and 0.3 for Figs. 4(*a*), 4(*b*), and 4(*c*), respectively. The results show that solutocapillary effects again partially stagnate the free surface. Surprisingly, thermocapillary effects are more pronounced at small x/L than was evident in the results of Fig. 2.

With a reduction in buoyancy forces, circulation rates and, in turn, advection from the hot wall to the cold wall are decreased. As a result, steeper temperature gradients exist along the free surface at small x/L for $Ra = 10^3$, relative to the results associated with $Ra = 10^4$. The locally steep free surface temperature gradients induce strengthened local thermocapillary effects and the host liquid is pulled to the surface near the upper hot wall. It is subsequently returned to smaller y/H as the vicinity of the stagnant free surface is approached. Hence, local thermocapillary forces become more influential in their role of pushing the surfactant to the cold wall.

Figure 5 includes the dimensionless free surface velocity and surfactant distributions associated with Fig. 4. A comparison with Fig. 3 shows that, due to enhanced local thermocapillary forces, a decrease in Ra leads to a reduction in the amount of the free surface stagnated by solutocapillary effects. Specifically, 20 percent reductions in the stagnant free surface length are noted. Again, this reduction is attributed to the enhanced pushing action of the buoyancy-enhanced thermocapillary forces at small x/L.

As evident in the results so far, the diffusing surfactant adjusts its distribution in response to advection induced by buoyancy and thermocapillary forces and stagnates a portion of the liquid's free surface. Hence a variation in Le may lead to a change in the system hydrodynamics (Bergman, 1986).

Figure 6 includes predicted dimensionless velocity and surfactant distributions at the free surface for $Ra = 10^4$, $Ma_T = 10^3$, $E = 0.1$, and Le = 1, 10, and 100. Variations in the

species diffusion rate wield little influence on the system response. The surfactant distribution is similar for all Le (distributions for Le = 10 and 100 coincide in the range $0.8 \le x/L \le 1.0$) and the surface velocity distribution is thermocapillary-dominated in the range $0.0 \le x/L \le 0.8$. Surface velocities in the range $0.8 \le x/L \le 1.0$ are very small and adjust in accordance with the predicted surfactant distribution and equation (5).

The insensitivity of the system response to Le is due to the tendency of the surfactant distribution to adjust in order to promote relative stagnation of the liquid surface adjacent to the cold wall. As long as surface velocities near the cold wall are small relative to the thermocapillary and buoyancy driven velocities throughout the remainder of the system, the temperature distribution remains nearly unchanged. Since the surfactant concentration distribution must continue to satisfy equation (6), it is relatively insensitive to variations in Le. As a result, the hydrodynamic and heat transfer phenomena associated with the host liquid are, for all practical purposes, unaffected by Le. It should be noted that, in the limit of Le = 0 ($D = \infty$), the influence of solutocapillary forces will be negligible. This range of Le was not examined, due to the limited number of real liquids (if any) characterized by $D = \infty$.

Heat Transfer Results. As evident from the previous discussions, inclusion of solutocapillary forces in the analysis leads to significant variations in the hydrodynamics of the system, especially in the vicinity of the free surface. Furthermore, system hydrodynamics are most profoundly influenced near the cold wall, which would correspond to the solid-liquid interface in a solidification or melting application. Hence, a consideration of the resulting impact on local and overall heat transfer rates across the host liquid layer is warranted.

Hot and cold wall Nu distributions associated with the simulations of Figs. 2-5 are presented in Fig. 7. Figure 7 (a) is associated with $Ra = 10^4$ and the free surface conditions of Fig. 3. Local heat transfer rates change as the surface conditions are varied and, as expected, the modifications in Nu are most severe at the upper cold wall. The local heat transfer rates are bracketed by results for the no-slip case and the situation where only thermocapillary forces are included in the analysis. As solutocapillary forces are increased, Nu is decreased at $y/H \cong 1.0$ and slightly increased below $y/H \cong 0.65$. The results for $E = 0.3$ are nearly identical to those associated with incorporation of no-slip boundary conditions.

Figure 7 (b) includes Nu distributions associated with $Ra = 10^3$ and the free surface conditions of Fig. 5 as well as $E = 0.0$ and no-slip cases. Again, the results are bracketed by the extreme cases of imposed no-slip free surface condition and the $E = 0$ results. In contrast to the results of Fig. 7 (a), slight differences exist between the $Ma = 10^3$, $E = 0.3$ and the no-slip results and are traceable to the decreased free surface stagnation length due to decreased buoyancy effects.

Finally, consideration is given to average cavity heat transfer rates in Fig. 8. Figure 8 (a) reports $\overline{Nu}$ for Le = 100 and $Ma_T = 10^3$ while Fig. 8 (b) shows $\overline{Nu}$ for Le = 100 and $Ma_T = 250$ for a range of Ra and E. As expected, the impact of surface tension forces on heat transfer is most severe at small Bo. At larger Bo, the condition of the free surface has little influence upon heat transfer in the system. Within the range of smaller Bo, solutocapillary effects systematically decrease heat transfer rates from the $E = 0$ results to the $E = \infty$ case, which corresponds to the imposition of no-slip boundary conditions at $y/H = 1$. It is noted that Bo values of order unity are common in many materials processing applications involving melting and solidification (Oreper and Szekely, 1984).

Summary and Conclusions

A numerical investigation has been conducted to identify and quantify phenomena that are responsible for the development of no-slip free surfaces in thermocapillary-affected

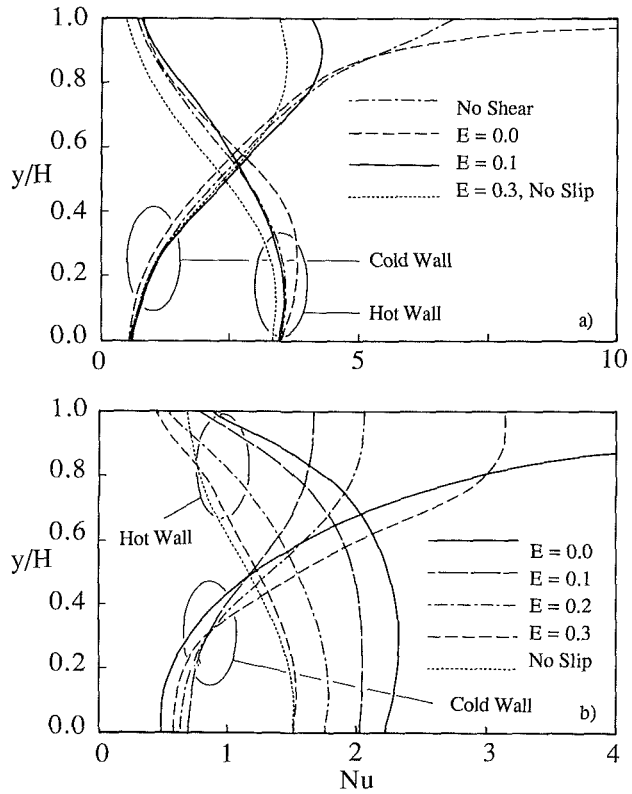

Fig. 7 Local hot and cold wall Nu distributions for (a) the predictions of Fig. 3 and (b) the predictions of Fig. 5

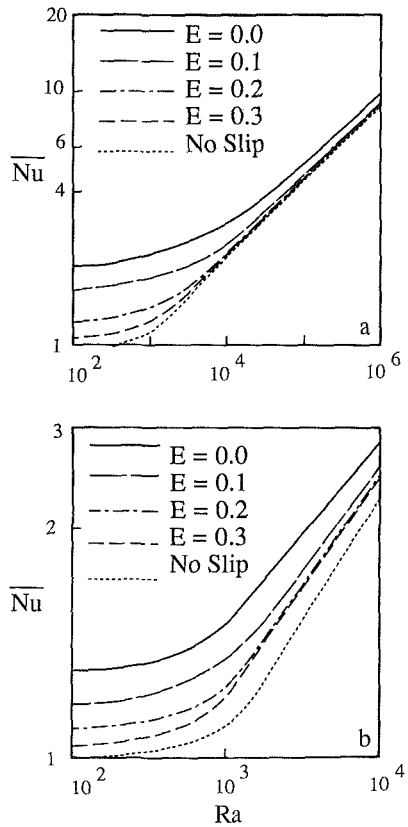

Fig. 8 Average heat transfer for various Ra and (a) $Ma_T = 10^3$ and (b) $Ma_T = 250$

flows. No-slip conditions are considered to be a third flow regime in combined buoyancy-thermocapillary flows and liquids that normally exhibit no slip boundary conditions are identified in the Appendix.

The hypothesis for no-slip boundary condition development is the counteracting role of solutocapillary forces in systems that may otherwise be thermocapillary-dominated. Surfactant concentration gradients develop along the free surface in response to bulk liquid motion and induce solutocapillary forces, which subsequently stagnate the free surface. Results show that variations in buoyancy, thermo-, and solutocapillary forces all affect the amount of free surface stagnation but variations in the species diffusion rate do not play a significant role.

The stagnating action of solutocapillary forces leads to reductions in the local and average heat transfer rates associated with thermocapillary-buoyancy convection. Decreases in the local heat transfer rate are most dramatic at the upper cold wall. Average heat transfer rates are decreased by solutocapillary forces for flows associated with small Bo.

Since the cold wall Nu distribution is most dramatically modified by thermo- and solutocapillary effects, the observed phenomena may be important in melting and solidification heat transfer. Furthermore, the role of solutal effects may be different in melting than in solidification since contaminants are often rejected from the solid phase during freezing, while species rejection is not an issue during melting. However, pure liquid issuing from a melting solid may reduce the surfactant concentration adjacent to the solid-liquid interface, allowing significant thermocapillary induced flow adjacent to the solid-liquid interface. Finally, if solidification of alloys is considered, the surfactant-induced solutocapillary effects may be overwhelmed by surface tension forces due, ultimately, to species rejection from the solid phase. Solutocapillary forces resulting from the presence of multiple species gradients along the free surface may, in fact, be common.

Acknowledgments

Support for this research by the National Science Foundation under grant No. CBT-8552806 is gratefully acknowledged. Computational facilities were provided by the Department of Mechanical Engineering at the University of Texas at Austin.

References

Bergman, T. L., 1986, "Numerical Prediction of Double-Diffusive Marangoni Convection," *Physics of Fluids*, Vol. 29, pp. 2103–2108.

Bergman, T. L., and Ramadhyani, S., 1986, "Combined Buoyancy- and Thermocapillary-Driven Convection in Open Square Cavities," *Numerical Heat Transfer*, Vol. 9, pp. 441–451.

Camel, D., Tison, P., and Favier, J. J., 1986, "Marangoni Flow Regimes in Liquid Metals," *Acta Astronautica*, Vol. 13, pp. 723–726.

Carpenter, B., and Homsy, G. M., 1985, "The Thermocapillary Flow in a Two-Dimensional Slot. Part 2, Partially Contaminated Interfaces," *Journal of Fluid Mechanics*, Vol. 155, pp. 429–439.

Chun, C. H., 1980, "Marangoni Convection in a Floating Zone Under Reduced Gravity," *Journal of Crystal Growth*, Vol. 48, pp. 600–610.

Davis, R. E., and Acrivos, A., 1966, "The Influence of Surfactant on the Creeping Motion of Bubbles," *Chemical Engineering Science*, Vol. 21, pp. 681–685.

De Vahl Davis, G., 1983, "Natural Convection of Air in a Square Cavity: A Bench Mark Numerical Solution," *International Journal of Numerical Methods in Fluids*, Vol. 3, pp. 249–261.

Heiple, C. J., and Roper, J. R., 1982, "Mechanism for Minor Element Effect on GTA Fusion Zone Geometry," *Welding Research*, Vol. 61, pp. 97s–102s.

Homsy, G. M., and Meiburg, E., 1984, "The Effect of Surface Contamination on Thermocapillary Flow in a Two-Dimensional Slot," *Journal of Fluid Mechanics*, Vol. 139, pp. 443–459.

Hurle, D. T. J., and Jakeman, E., 1981, "Introduction to the Techniques of Crystal Growth," *Physico Chemical Hydrodynamics*, Vol. 2, pp. 237–244.

Kirdyashkin, A. G., 1984, "Thermogravitational and Thermocapillary Flows in a Horizontal Liquid Layer Under the Conditions of a Horizontal Temperature Gradient," *International Journal of Heat and Mass Transfer*, Vol. 27, pp. 1205–1218.

Kou, S., 1987, *Welding Metallurgy*, Wiley, New York.

Legros, J. C., Limbourg-Fontaine, M. C., and Petre, G., 1984, "The Influence of a Surface Tension Minimum as a Function of Temperature on the Marangoni Convection," *Acta Astronautica*, Vol. 11, pp. 143–147.

Levich, V. G., 1962, *Physicochemical Hydrodynamics*, Prentice-Hall, Englewood Cliffs, NJ.

Levich, V. G., and Krylov, V. S., 1969, "Surface Tension Driven Phenomena," *Annual Review of Fluid Mechanics*, Vol. 1, pp. 293–316.

McNeil, T. J., Cole, R., and Subramanian, R. S., 1985, "Surface Tension Driven Flow in a Glass Melt," *Journal of the American Ceramics Society*, Vol. 68, pp. 254–259.

Patankar, S. V., 1980, *Numerical Heat Transfer and Fluid Flow*, Hemisphere Publishing Corp., Washington, DC.

Platten, J. K., and Villers, D., 1987, "On Thermocapillary Flows in Containers With Differentially Heated Side Walls," *Proceedings of the NATO Advanced Study Institute at La Rabida*, Plenum Press, New York.

Oreper, G., and Szekely, J., 1984, "Heat- and Fluid-Flow Phenomena in Weld Pools," *Journal of Fluid Mechanics*, Vol. 147, pp. 53–79.

Savic, P., 1953, "Circulation and Distortion of Liquid Drops Falling Through a Viscous Medium," Report No. MT-22, Division of Mechanical Engineering, National Research Council of Canada.

Schwabe, D., Scharmann, A., Presser, F., and Oeder, R., 1978, "Experiments on Surface Tension Driven Flow in Floating Zone Melting," *Journal of Crystal Growth*, Vol. 43, pp. 305–312.

Shinoda, K., 1963, *Colloidal Surfactants*, Academic Press, New York.

Stanek, V., and Szekely, J., 1970, "The Effect of Surface Driven Flows on the Dissolution of a Partially Immersed Solid in a Liquid—Analysis," *Chemical Engineering Science*, Vol. 25, pp. 699–715.

Villers, D., and Platten, J. K., 1985, "Marangoni Convection in Systems Presenting a Minimum in Surface Tension," *Physico Chemical Hydrodynamics*, Vol. 6, pp. 435–451.

Zehr, R. L., Chen, M. M., and Mazumder, J., 1987, "Thermocapillary Convection of a Differentially Heated Cavity at High Marangoni Numbers," presented at the National Heat Transfer Conference, Pittsburgh, Paper No. 87-HT-29.

APPENDIX

Experiments have been performed to visualize the flows of regimes 1 and 3 qualitatively and to categorize the propensity of various fluids to exhibit the flow of a particular regime.

A test cell was constructed using multipass copper heat exchangers to impose isothermal boundary conditions on the sides of the test fluid. The side walls were separated by 10 mm to insure a small Bo and, in turn, induce substantial thermocapillary effects, relative to buoyancy. Two-dimensional flow was approximated by making the test cell deep relative to its width (65 mm). An air gap of approximately 2 mm was placed above the liquid layer to minimize evaporation and convection effects.

The test fluid was seeded with aluminum particles and illuminated with a vertical sheet of laser light. Time exposure photography was used to visualize streamlines.

The surfactant in question is absorbed from the environment or leached from test cell components. As such, its composition and average concentration are unknown. In order to illustrate the tendency of common fluids to exhibit the flow of

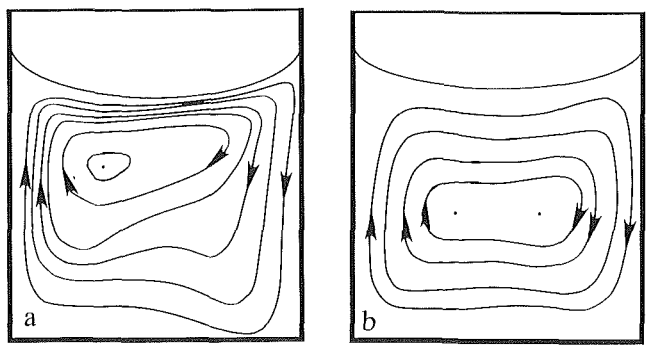

Fig. 9 Experimentally observed streamlines for (*a*) ethanol and (*b*) water

regime 3, precautions were taken to avoid contamination of the host liquid and included: (1) covering all interior surfaces of the test cell with teflon or glass, (2) ultrasonically cleaning the test cell for four hours, and (3) triple rinsing with triple-distilled water prior to each flow visualization experiment.

Figure 9 shows streamlines for ethanol and water, which were sketched from the photographs. (The original photographs are not presented since the free surface curvature causes local overexposure of the film and their quality is poor.) Each condition is characterized by $Ra = 10^5$ and Ma_T values of 1.4×10^4 and 1.0×10^4 for ethanol and water, respectively. The value of E is unknown.

Ethanol (Fig. 9*a*) clearly exhibits regime 1 flow as the center of rotation is above $y/H = 0.5$, implying relatively large free surface velocities. As is well known, however, water (Fig. 9*b*) exhibits regime 3 flow as the center of rotation is at $y/H = 0.5$.

Table 1 summarizes the tendency of various host liquids to fall into a specific flow regime. Entries in the table without references were identified experimentally and the appearance of a fluid in multiple regimes indicates that extreme precautions (beyond those taken here) are necessary to avoid regime 3 behavior.

Table 1 Regime behavior of various liquids

Regime 1	Regime 2	Regime 3
Water above 4°C[a]	Water below 4°C[a]	Water
Fluorocarbons	Aqueous alcohol solutions[f]	*n*-Octadecane
Sodium nitrate[b]	Binary metal alloys[e]	*n*-Hexadecane
Silicon oil[c]		Decanol
Molten glass[d]		
Molten tin[e]		

[a]Platten and Villers, 1987.
[b]Schwabe et al., 1978.
[c]Chun, 1980.
[d]McNeil et al., 1985.
[e]Camel et al., 1986.
[f]Legros et al., 1984.